View metadata, citation and similar papers at core.ac.uk

brought to you by CORE

provided by Birkbeck Institutional Research Online

Anomaly Detection Using Local Kernel Density Estimation and Context-Based Regression

Weiming Hu, Jun Gao, and Bing Li
(National Laboratory of Pattern Recognition, Institute of Automation, Chinese Academy of Sciences, Beijing 100190)
{wmhu, jgao, bli}@nlpr.ia.ac.cn

Ou Wu
(Center for Applied Mathematics, Tianjin University, Tianjin 300073)
wuou@tju.edu.cn

Junping Du
(School of Computer Science, Beijing University of Posts and Telecommunications, Beijing 100876)
junpingdu@126.com

Stephen Maybank
(Department of Computer Science and Information Systems, Birkbeck College, Malet Street, London WC1E 7HX)
sjmaybank@dcs.bbk.ac.uk

Abstract: Current local density-based anomaly detection methods are limited in that the local density estimation and the neighborhood density estimation are not accurate enough for complex and large databases, and the detection performance depends on the size parameter of the neighborhood. In this paper, we propose a new kernel function to estimate samples' local densities and propose a weighted neighborhood density estimation to increase the robustness to changes in the neighborhood size. We further propose a local kernel regression estimator and a hierarchical strategy for combining information from the multiple scale neighborhoods to refine anomaly factors of samples. We apply our general anomaly detection method to image saliency detection by regarding salient pixels in objects as anomalies to the background regions. Local density estimation in the visual feature space and kernel-based saliency score propagation in the image enable the assignment of similar saliency values to homogenous object regions. Experimental results on several benchmark datasets demonstrate that our anomaly detection methods overall outperform several state-of-art anomaly detection methods. The effectiveness of our image saliency detection method is validated by comparison with several state-of-art saliency detection methods.

Index terms: Anomaly detection, Local kernel density estimation, Weighted neighborhood density, Hierarchical context-based local kernel regression

1. Introduction

The task of anomaly (novelty, outlier, or fault) detection [1, 2, 3, 18, 25, 29, 30, 40, 52, 53, 54, 55, 57, 58, 59] is to find abnormal data, rare events, or exceptional cases in large datasets. Anomalies [4, 5] in datasets may contain very important information, even possibly inspiring new perspectives, theories, or discoveries. Anomaly detection has a wide range of applications, such as visual surveillance [24], detection of abnormal regions in images, industrial damage detection, medical diagnostics, protein sequence analysis, irregularity finding in gene expressions, commercial fraud detection, stock market analysis, communication embezzlement detection, social network graph search, and network intrusion detection. Anomaly detection has attracted much attention, and many attempts have been made for it.

1.1. Related work

Anomaly detection methods are classified as supervised, if labeled training samples are available, otherwise they are classified as unsupervised. If only a few labeled samples are available, then they may not meet the requirements for detecting anomalies in very large datasets. In particular, it may not be possible to detect the types of anomalies which do not appear in the training dataset. Unsupervised methods do not require labeled samples, but they usually make assumptions about the data. When the data do not match the assumptions, a high false alarm rate occurs.

According to the assumptions made and the choice of algorithms, anomaly detection methods can be classified into statistical model-based, classifier-based, clustering-based, beyond supervised and unsupervised, and local density-based.

1) Statistical model-based: These methods construct distribution models for samples, and detect anomalies which do not match the models. Supervised methods model the distributions of normal samples and/or anomalies. Unsupervised methods model the distribution of all the samples and regard samples in the sparse regions as anomalies. The statistical models include

- non-parametric models, such as histograms [31] and the Parzen windows-based models [32],
- parametric models [26], such as the Gaussian distribution [33], the Poisson distribution, the Markov chain model [34], and the mixture statistical model [35].

Statistical model-based methods are effective in detecting anomalies in low dimensional datasets. But, statistical models are not effective enough in describing the large high-dimensional complex datasets.

2) Classifier-based: These methods usually detect anomalies using classifiers constructed from labeled samples [28]. For instance, Jumutc and Suykens [23] detected anomalies using **a** multi-class classifier. These methods are appropriate for the applications in which anomalous samples are not difficult to obtain. There are also some methods for constructing classifiers in an unsupervised way, i.e., by transforming unsupervised detection to supervised detection. For instance, Markou and Singh [27] proposed a neural network-based method for anomaly detection using normal samples and artificially generated anomalies. Stein et al [51] detected anomalies in the process of constructing a random decision tree classifier. The original classifier-based methods require labeled anomalous samples and normal samples. The methods which construct classifiers in an unsupervised way lack solid theoretical support and extendable learning frameworks.

3) Clustering-based: These methods detect anomalies after clustering the samples. The samples not belonging to any cluster, the samples far from the cluster centers, and the samples in very sparse or small clusters [36, 38] are treated as isolated anomalies, edge anomalies, and sparsely clustered anomalies, respectively. Yu et al. [37] applied a wavelet transformation to the quantized feature space and found sample clusters in this space. The clusters were removed and then the anomalies were identified. He et al. [39] applied the Squeezer clustering algorithm to estimate samples' local anomaly factors which were used to detect anomalies. Shah et al. [65] proposed an excellent information theoretic method for general node-based anomaly detection in edge-attributed graphs. They leveraged minimum description length to rank abnormality of nodes in an unsupervised way. Wu et al. [67] explicitly modeled temporal patterns of users' review behaviors using a probabilistic generative model, and modeled users' review credibility and objects' highly-skewed review distributions for reliable fake review detection. The merit of the clustering-based methods is that they are unsupervised. Their limitations are that they have high computational complexity, and the anomalous samples may affect the clustering, leading to reduced performance.

4) Beyond supervised and unsupervised: There are anomaly detection methods beyond supervised and unsupervised, such as semi-supervised learning-based and active learning-based. Semi-supervised methods, including semi-supervised classification and semi-supervised clustering, utilize both unlabeled and labeled samples to find anomalies. A good semi-supervised method is belief propagation [62, 63, 64] which iteratively propagates the information from a few nodes with explicit labels to a whole network. Pandit et al. [62] employed a belief propagation mechanism to detect likely abnormal sub-graphs in the full graph. The maximum likelihood state probabilities of nodes were inferred, given that the correct states for some nodes are known. Chau et al. [63] leveraged the labels of the known normal and known abnormal samples in the graph to infer unknown labels. Abe et al. [14] presented an active learning-based method for anomaly detection by classifying the artificially generated anomalies and the normal samples taken from the dataset. A selective sampling mechanism based on active learning was employed to provide improved accuracy for anomaly detection. Li et al. [66] proposed a semi-supervised method for social spammer detection. A classifier with a small number of labeled data was trained. A ranking model was used to propagate trust and distrust. Yuan et al. [68] proposed an intrusion detection framework, using tri-training with three different Adaboost algorithms. This framework combines the ensemble-based and semi-supervised learning methods. The methods beyond supervised and unsupervised improve the accuracy of anomaly detection using supervision of a small number of labeled samples in contrast with unsupervised learning, while reducing the need for a large number of labeled samples required for supervised learning. Their limitation is that anomaly detection has to be customized to specific application domains in which only some of the samples are labeled.

5) Local density-based: These methods [8, 10, 11, 12, 13, 17] detect anomalies by analyzing contexts between samples and the densities of their neighbors. In contrast with the clustering-based methods which detect anomalies from a global perspective [19, 22], the local density-based methods detect anomalies by analyzing the sample distribution in the neighborhood of a given sample from a local perspective. The local density-based methods are classified into DBSCAN (the density-based spatial clustering of applications with noise)-based, neighborhood radius-based, local anomaly factor-based, local correlation integral-based, and local peculiarity factor-based:

- **The DBSCAN-based methods [60, 61]** divide samples into core, reachable, and abnormal. A sample *p* is a core sample if at least a fixed number of samples are within a fixed radius of *p*. Those samples are said to be directly reachable from *p*. A sample *q* is directly reachable from *p* if *q* is within a fixed radius of *p* and *p* is a core sample. A sample *q* is reachable from *p* if there is a path linking *p* and *q*, and all the samples on the path are core ones, with the possible exception of *q*. All the samples not reachable from any other samples are anomalies. The DBSCAN-based methods cannot detect anomalies reliably in datasets with large differences in densities.
- **The neighborhood radius-based methods** use the distance [41] between a given sample and its *k*-th nearest neighbor (the neighborhood radius of the sample) to decide if the sample is anomalous. Given a fixed value of *k*, the larger this distance, the sparser the distribution of the samples and the more likely it is that the given sample is an anomaly. The neighborhood radius-based methods are not well adapted to datasets in which denseness and sparseness of distributions of samples are mixed very irregularly.

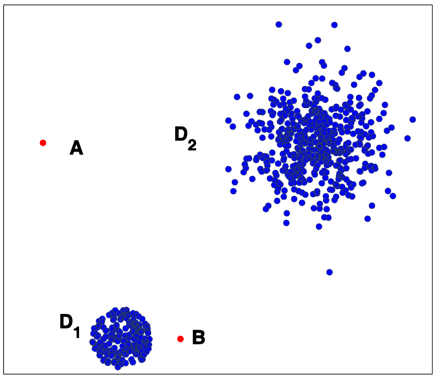

Fig. 1. An example to show the advantage of the local density estimation-based anomaly detection method over the neighborhood radius-based method.

- **Local anomaly factor-based methods** use the ratio of the neighborhood density of a given sample, measured using the local densities of the neighbors of the sample, to the local density of the sample to determine the anomaly factor of the sample [7]. The less the local density of a sample and the larger its neighborhood density, the larger the anomaly factor of the sample. The local anomaly factors for normal samples fluctuate around 1 and the local anomaly factors for anomalies are much larger than 1. This can distinguish anomalies from normal samples more clearly. Fig. 1 shows an example that the local anomaly factor-based methods have advantages in contrast with the neighborhood radius-based methods. In the figure, the blue points represent normal samples distributed in the denser cluster D_1 and the less dense cluster D_2. The red points A and B represent anomaly samples which are isolated from the two clusters. Anomaly A is detected by both the neighborhood radius-based method and the local density estimation-based method. Anomaly B is close to cluster D_1, and is not detected using only the neighborhood radius. As the neighborhood density of Anomaly B is high, it is easily detected by the local density estimation-based method. Latecki et al. [9] proposed a typical local anomaly factor-based anomaly detection method. They used the Gaussian kernel to estimate local densities of samples. The shape of the whole neighborhood was adjusted using the covariance matrix of the Gaussian. The limitations of Latecki et al's work [9] are that the influence of the size of the neighborhood is not considered and the global properties of the distribution of the samples are ignored. Schubert et al. [56] formulated an excellent generalization of a density-based anomaly detection method based on kernel density estimation. They applied the z-score transformation to standardize the deviation from normal density. The normal cumulative density function was used to normalize the scores to the range [0, 1], and then a rescaling was applied to obtain the anomaly score. Schubert et al.'s method [56] has flexible applicability and scalability.

- **The local correlation integral-based methods [8]** use the number of neighbors in a fixed radius of a sample to measure the local density of the sample. The distance between the Gaussian distributions of the local density of a given sample and the local densities of its neighbors is used as the anomaly factor of the sample. For a given sample, the maximum of the anomaly factors obtained using different neighborhood radiuses is used to measure the possibility that the sample is an anomaly. These methods avoid the choice of the neighborhood size *k*, but require more computational cost.
- **The local peculiarity factor-based methods [10]** compute the anomaly factors for each feature dimension and the weighted average of these anomaly factors for a sample is used as the final anomaly factor for the sample. The computational complexity has a direct correlation with the number of dimensions of feature vectors. Therefore, these methods are not adapted to high-dimensional datasets.

The local density-based methods [20] are unsupervised and can be applied to complex datasets with sparse or dense mixed samples of different types. However, overall the current local density-based methods have the following common limitations:

- Local density estimation is not accurate enough, which leads to a reduced performance.
- Their performance depends on the choice of the neighborhood size parameter.
- These methods are based on local analysis. The global properties of the distribution of the samples are ignored.

1.2. Our work

In this paper, we focus on local density-based anomaly detection, aiming at removing the above limitations in local density estimation-based anomaly detection. We propose a new anomaly factor estimation method which uses the ratio of the weighted neighborhood density to the local kernel density of a sample as the anomaly factor of the sample and uses hierarchical context-based local regression to refine the anomaly factors of each sample. The main contributions of our work are summarized as follows:

- We propose a new kernel function**,** the Volcano kernel, which is more appropriate for estimating the local densities of samples and then detecting anomalies.
- We propose a weighted neighborhood density estimation which is more robust to the neighborhood size parameter than the traditional averaged neighborhood density estimation.
- We propose a multi-scale local kernel regression method together with a new context-based kernel function to combine the information from multiple scale neighborhoods for locally and globally refining the samples' anomaly factors.
- We apply the proposed general anomaly detection methods to image saliency detection, based on local density estimation of visual features and saliency score propagation in the image. Our method uniformly highlights entire salient regions in contrast with previous methods which only produce high saliency scores at or near object edges [49, 50].

The remainder of this paper is organized as follows: Section 2 proposes our anomaly detection method based on local kernel and weighted neighborhood density. Section 3 presents our anomaly factor refinement method based on the hierarchical context-based kernel regression. Section 4 applies our anomaly detection methods to image saliency detection. Section 5 reports the experimental results. Section 6 concludes the paper. Table 1 clarifies notations in the paper, helping keep track of symbols' meaning.

Table 1. Symbol Table

Symbols	Descriptions
D	A dataset.
d	The dimension of samples in a dataset.
$\mathbf{p}$	A *d*-dimensional sample in *D*.
x_i	The *i*-th element in p
$d_k(\mathbf{p})$	The *k*-distance of p.
$d(\mathbf{p},\mathbf{o})$	The distance between samples p and o.
$N_k(\mathbf{p})$	The *k*-distance neighborhood of p.
$\pi(\mathbf{p})$	The nearest neighbor density estimation for sample p.
$K(\mathbf{z})$	A multivariate kernel function for a variable z.
$f(\mathbf{q})$	A prior density for sample **q**.
g	The geometric mean of $\{f(\mathbf{q})\}_{\mathbf{q}\in N_k(\mathbf{p})}$.
$\lambda_{\mathbf{q}}$	The local bandwidth factor.
α	The sensitivity parameter for the local bandwidth factor.
$kde(\mathbf{p})$	The local kernel density estimation of sample **p.**
H	The smoothing parameter for the local kernel density estimation.
γ	The sensitivity parameter for the local kernel density estimation.
$\mathbf{z}$	A random variable vector.
β	The kernel parameter.
$\omega_{\mathbf{q}}$	The weight of sample **q** in a *k*-distance neighborhood.
$wde(\mathbf{p})$	The weighted neighborhood density for sample **p.**
σ	A positive scaling factor.

$WAF(\mathbf{p})$	The weighted anomaly factor for a sample **p.**
N	The number of samples in a dataset.
$\mathbf{x}_i$	The *i*-th sample in the dataset.
y_i	The estimated anomaly factor for $\mathbf{x}_i$ **.**
$\boldsymbol{t}$	The iteration step index.
$\mathbf{c}_j$	The value vector of pixel *j* in the CIE L*a*b* color space.
I_i	The image patch centered at pixel *i*.
$\mathbf{v}_i$	A feature vector describing I_i
ω_j	The weight for pixel *j*.
$d_{spatial}(i, j)$	The Euclidean distance between positions of pixels *i* and *j*.
$S(i)$	The saliency score for pixel *i*.
L	An image multi-scale set.

2. Local Kernel Density-Based Anomaly Detection

A density estimation-based method detects anomalies by comparing the density of each sample with its neighborhood density which is usually the average of the local densities of its neighbors [7]. We propose a new kernel function for local density estimation and a weighted neighborhood density to calculate each sample's anomaly factors which are used to detect anomalies. Our anomaly detection method based on the weighted neighborhood density is robust to the neighborhood size parameter.

2.1. Definition of neighborhood

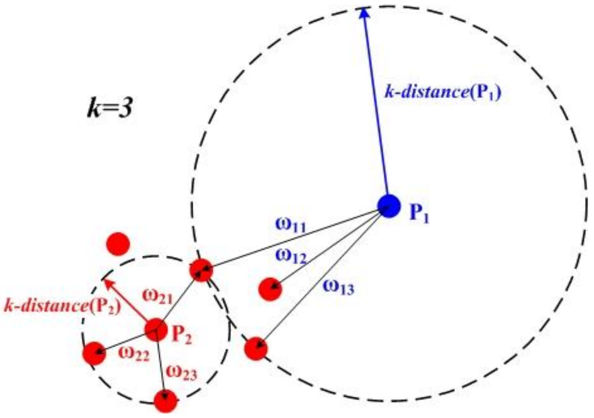

Fig. 2. 3-distance neighborhoods.

Let D be a dataset and let $|D|$ be the number of the samples in D. Let $\mathbf{p} = [x_1, x_2, ..., x_d]$ be a d-dimensional sample in D. For any positive integer k ($k \le |D|$), the k-distance $d_k(\mathbf{p})$ of $\mathbf{p}$ is defined as the distance $d(\mathbf{p}, \mathbf{o})$ between $\mathbf{p}$ and a sample $\mathbf{o} \in D$, such that in $D \setminus \{\mathbf{p}\}$

- there are at least k samples $\mathbf{q}$ of which holds that $d(\mathbf{p}, \mathbf{q}) \le d(\mathbf{p}, \mathbf{o})$,
- there are at most k-1 samples $\mathbf{q}$ of which holds that $d(\mathbf{p}, \mathbf{q}) < d(\mathbf{p}, \mathbf{o})$.

The k-distance neighborhood of $\mathbf{p}$, denoted as $N_k(\mathbf{p})$, contains the samples whose distances from $\mathbf{p}$ are not larger than the k -distance of $\mathbf{p}$: $N_k(\mathbf{p})=\{\mathbf{q}\in D\backslash\{\mathbf{p}\}\,|\,d(\mathbf{p},\mathbf{q})\le d_k(\mathbf{p})\}$. Any sample $\mathbf{q}$ in $N_k(\mathbf{p})$ is called a *k*-distance neighbor of **p**. In Fig. 2, the red points are normal samples and the blue point is an anomaly. In particular, the point $\mathbf{p_2}$ is a normal sample and the point $\mathbf{p_1}$ is an anomaly. The 3-distance neighborhood of p_2 is obviously less than the 3-distance neighborhood of p_1, i.e., *k*-distance($\mathbf{p_2}$)<*k*-distance($\mathbf{p_1}$). The size of the *k*-distance neighborhood of a sample in the space has an inverse relation to the local density of the sample. Given *k*, the denser the samples, the smaller the *k*-distances of these samples.

2.2. Local kernel density estimation

The density estimation methods in common use include histogram-based, nearest neighbor-based, and kernel-based methods [6]. The histogram-based density estimation is simple to implement and has a low time complexity. But its distribution density is discrete (not a smooth curve) and it is seldom used for anomaly detection. The nearest neighbor density estimation is defined as:

$$\pi(\mathbf{p})=\frac{k}{2|D|}\cdot\frac{1}{d_k(\mathbf{p})}\,. \tag{1}$$

The limitations of the distribution curve yielded by the nearest neighbor density estimation are that the curve is not smooth and **the** integral over it does not equal to 1 [6]. As shown in Fig. 3, the heavy tails of the density function and the discontinuities in the derivative for the nearest neighbor density estimate reduce the accuracy of the density estimate. This reduction may lead to an increase in errors of anomaly detection for complex and large databases. By using kernel functions, the kernel density estimate yields a smooth distribution curve over which the integral equals 1. The size of the window can be used to adjust the smoothness of the curve.

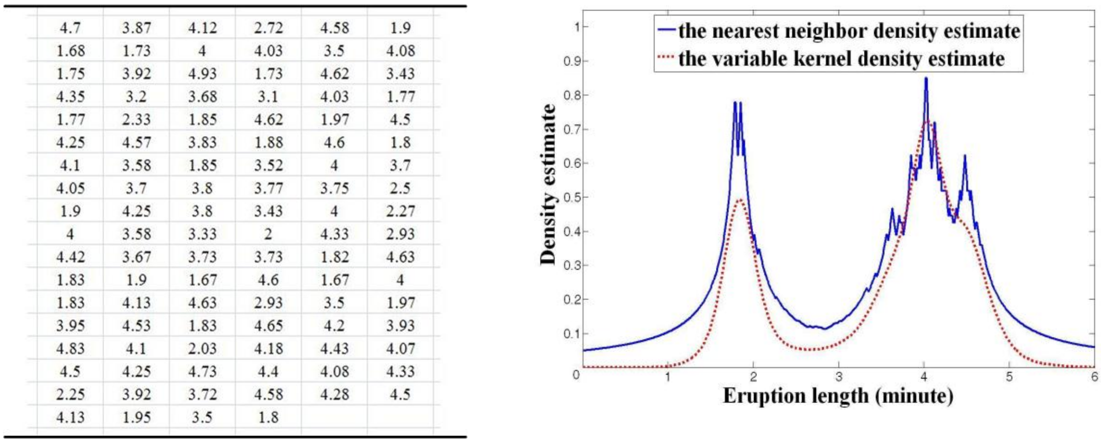

4.7	3.87	4.12	2.72	4.58	1.9
1.68	1.73	4	4.03	3.5	4.08
1.75	3.92	4.93	1.73	4.62	3.43
4.35	3.2	3.68	3.1	4.03	1.77
1.77	2.33	1.85	4.62	1.97	4.5
4.25	4.57	3.83	1.88	4.6	1.8
4.1	3.58	1.85	3.52	4	3.7
4.05	3.7	3.8	3.77	3.75	2.5
1.9	4.25	3.8	3.43	4	2.27
4	3.58	3.33	2	4.33	2.93
4.42	3.67	3.73	3.73	1.82	4.63
1.83	1.9	1.67	4.6	1.67	4
1.83	4.13	4.63	2.93	3.5	1.97
3.95	4.53	1.83	4.65	4.2	3.93
4.83	4.1	2.03	4.18	4.43	4.07
4.5	4.25	4.73	4.4	4.08	4.33
2.25	3.92	3.72	4.58	4.28	4.5
4.13	1.95	3.5	1.8		

(a) Old Faithful data

(b) Density estimate

Fig. 3. (a) The lengths of 107 eruptions of Old Faithful geyser; (b) The density of Old Faithful data based on the nearest neighbor density estimate, redrawn from [6].

We extend the standard kernel density estimation [6] to a type of local kernel density estimation and propose to use **the** local kernel density to estimate the local densities of samples. Let $K(\mathbf{z})$ be a multivariate kernel function for a variable vector **z**. Let $f(\mathbf{q})$ be a prior density for sample **q**. Let *g* be the geometric mean of $\{f(\mathbf{q})\}_{\mathbf{q}\in N_k(\mathbf{p})}$:

$$g = \exp\left(\frac{\sum_{\mathbf{q}\in N_k(\mathbf{p})} \log\left(f(\mathbf{q})\right)}{\left|N_k(\mathbf{p})\right|} \right) \tag{2}$$

where $\left|N_k(\mathbf{p})\right|$ is the number of the *k*-distance neighbors of **p**. Let $\lambda_{\mathbf{q}}$ be the local bandwidth factor: $\lambda_{\mathbf{q}} = (f(\mathbf{q})/g)^{-\alpha}$, where α is the sensitivity parameter that satisfies $o \le \alpha \le 1$. The local kernel density estimation of a sample **p** is defined as:

$$kde(\mathbf{p}) = \frac{\sum_{\mathbf{q}\in N_k(\mathbf{p})} \left\{ h^{-\gamma}\lambda_{\mathbf{q}}^{-\gamma} K\left(h^{-1}\lambda_{\mathbf{q}}^{-1}(\mathbf{p}-\mathbf{q})\right)\right\}}{\left|N_k(\mathbf{p})\right|} \tag{3}$$

where *h* is the smoothing parameter and γ is the sensitivity parameter. We explain the following points with respect to (3):

- As in traditional kernel density estimation, the local kernel density estimation adaptively adjusts the kernel window size from one sample to another according to the value of $\lambda_{\mathbf{q}}$.
- The $kde(\mathbf{p})$ is computed locally in the *k*-distance neighborhood of sample **p**, rather than in the entire dataset for the traditional kernel density estimation. Therefore, the computational complexity is greatly reduced.
- In the traditional kernel density estimation [6], the parameter γ is set to the dimension *d* of the sample feature vectors. For the local kernel density estimation, a large value of γ may make $kde(\mathbf{p})$ unstable or sensitive. For example, if $\lambda_{\mathbf{q}}$ is very small, then $(\lambda_{\mathbf{q}})^{-\gamma}$ approximates infinity. We experimentally determine an appropriate value of γ as $\gamma = 2$ using cross verification to maintain a balance between sensitivity and robustness.
- In $kde(\mathbf{p})$, the window adjustment parameter $\lambda_{\mathbf{q}}$ depends on the prior density function $f(\mathbf{q})$. It is required that $f(\mathbf{q})$ can, overall, contrast local densities of different samples. As the *k*-distance of **q** is inversely related to the local density of **q**, we estimate $f(\mathbf{q})$ as follows:

$$f(\mathbf{q}) = \frac{1}{d_k(\mathbf{q})}. \tag{4}$$

We substitute (4) into (3), and then the local kernel density of sample **p** becomes:

$$kde(\mathbf{p}) = \frac{\sum_{\mathbf{q}\in N_k(\mathbf{p})} \frac{1}{(C\cdot d_k(\mathbf{q})^{\alpha})^2} K\left(\frac{\mathbf{p}-\mathbf{q}}{C(d_k(\mathbf{q}))^{\alpha}}\right)}{\left|N_k(\mathbf{p})\right|} \tag{5}$$

where $h = C/g^{\alpha}$. The default value of α is 1.

2.3. Kernel function

The kernel function **in (5)** is very important for density estimation. The multivariate Gaussian function and the Epanechnikov kernel function are commonly used in the kernel density estimation. However, the Gaussian kernel and the Epanechnikov kernel are not appropriate for use in (5). Therefore, we define a new kernel function which is more appropriate for our kernel-based anomaly factor method to detect anomalies.

The multivariate Gaussian kernel function is defined as:

$$K(\mathbf{z}) = (2\pi)^{-d/2} \exp\left(-\frac{1}{2}\|\mathbf{z}\|^2\right) \tag{6}$$

where $\|\mathbf{z}\|$ denotes the Euclidean norm of a variable vector **z**. The Epanechnikov kernel function is defined as:

$$K(\mathbf{z}) = \begin{cases} (3/4)^d (1-\|\mathbf{z}\|^2), & \mathit{if}\ \|\mathbf{z}\| \le 1 \\ 0, & \mathit{otherwise} \end{cases}. \tag{7}$$

Fig. 4 shows the curves of the Gaussian kernel and the Epanechnikov kernel. The traditional local density-based anomaly detection methods, which usually use the ratio of its neighborhood density to its local density as its anomaly factor, have the advantage that the obtained anomaly factors of normal samples fluctuate around “1” and the obtained anomaly factor values of anomalies are obviously larger than “1”. But, if the Gaussian kernel is used for estimating anomaly factors, it is not guaranteed that the anomaly factors of normal samples within a cluster are approximately equal to 1. This makes it difficult to determine the threshold value for anomaly factors. As shown in Fig. 4, the Epanechnikov kernel function equals zero when $\|\mathbf{z}\|$ is larger than 1. If the Epanechnikov kernel is used for estimating anomaly factors, most of anomalies and normal samples lying in the borders of clusters have anomaly factors equal to infinity. This influences the results of anomaly detection.

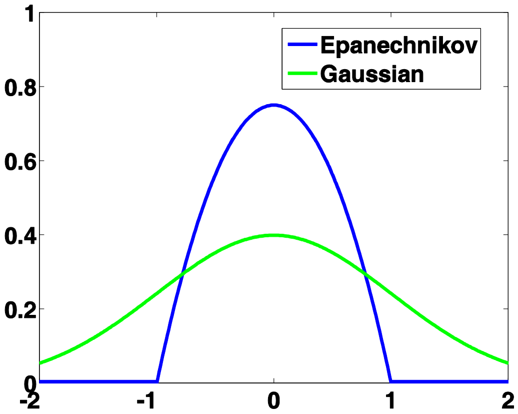

Fig. 4. The shapes of the curves of the Gaussian kernel and the Epanechnikov kernel.

In order to avoid the limitations in using the Gaussian kernel and the Epanechnikov kernel for estimating anomaly factors, we propose a new kernel function, the Volcano kernel, which is defined as:

$$K(\mathbf{z})=\begin{cases}\beta, & if\ \|\mathbf{z}\|\le 1\\ \beta\xi(\|\mathbf{z}\|), & otherwise\end{cases} \tag{8}$$

where β is chosen such that $K(\mathbf{z})$ integrates to one, and $\xi(\|\mathbf{z}\|)$ is a monotonically decreasing function taking values in the closed interval $[0,1]$ and tending to zero at the infinity. We use $\xi(\|\mathbf{z}\|)=\exp(-\|\mathbf{z}\|+1)$ as the default function. The mathematical derivation of β is included in Appendix A. Fig. 5 shows the curve of our Volcano kernel function in a univariate feature space. When $\|\mathbf{z}\|\le 1$, the kernel value equals a constant β. This ensures that the anomaly factors of the samples within a cluster approximate to 1. When $\|\mathbf{z}\|>1$, the kernel value is less than 1 and monotonically decreases as $\|\mathbf{z}\|$ increases. This makes the anomaly factors of anomalies much larger than 1. Hence, the proposed kernel function is suitable for anomaly detection.

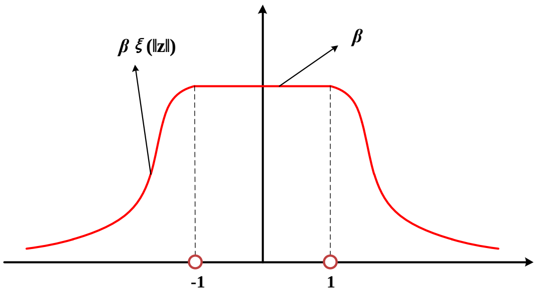

Fig. 5. The curve of the proposed Volcano kernel function in a univariate feature space.

The neighborhood size *k* needed by our Volcano kernel is less than the neighborhood size *k* needed by the Gaussian kernel and the Epanechnikov kernel. The reason is that the Gaussian kernel and the Epanechnikov kernel are designed to estimate the distribution densities of samples. The larger the value of *k*, the more samples are involved in density estimation and the more accurate the density estimate. However, our Volcano kernel is specifically designed to detect anomalies. Its motivation is to make the anomaly factors of normal samples approximate to 1 and the anomaly factors of anomalies much larger than 1. The values of the random variable $\|\mathbf{z}\|$ for normal samples, which are the majority of the samples in the dataset, lie between -1 and 1. For our Volcano kernel, only a line segment is used to represent the densities when $\|\mathbf{z}\|$ is within [-1,1] as shown in Fig. 5, while a curve segment is used for the Gaussian kernel or the Epanechnikov kernel as shown in Fig. 4. It is apparent that estimation of the density of a sample using the Volcano kernel requires fewer neighboring samples than estimation using the Gaussian kernel or the Epanechnikov kernel. Therefore, our Volcano kernel requires a smaller neighborhood size *k*.

2.4. Weighted neighborhood density

The performance of local density-based anomaly detection depends strongly on the choice of an appropriate value of the neighborhood parameter *k*. Only when *k* is large enough such that most of the samples in the neighborhood are normal, can the anomalies be detected. In order to increase the robustness to the parameter *k*, we propose a weighted neighborhood density, in contrast with the traditional neighborhood density which is the average of the local densities of all the neighbors of a sample and is sensitive to the presence of anomalies in the neighborhood.

The weighted neighborhood density $wde(\mathbf{p})$ is defined for a sample **p** as follows:

$$wde(\mathbf{p}) = \frac{\sum_{\mathbf{q}\in N_k(\mathbf{p})} \omega_{\mathbf{q}} \cdot kde(\mathbf{q})}{\sum_{\mathbf{q}\in N_k(\mathbf{p})} \omega_{\mathbf{q}}} \tag{9}$$

where $\omega_{\mathbf{q}}$ is the weight of sample **q** in the *k*-distance neighborhood of sample **p**. The weight $\omega_{\mathbf{q}}$ is inversely related to the *k*-distance of **q**, and we define it as follows:

$$\omega_{\mathbf{q}} = \exp\left(-\frac{\left(\frac{d_k(\mathbf{q})}{min_k} - 1\right)^2}{2\sigma^2} \right) \tag{10}$$

where σ is a positive scaling factor and

$$min_k = \min_{\mathbf{q}\in N_k(\mathbf{p})} (d_k(\mathbf{q})) . \tag{11}$$

The weight of a neighboring sample is a monotonically decreasing function of its *k*-distance. The neighboring sample with the smallest *k*-distance has the largest weight which equals 1. Other neighbors' weights lie within interval (0,1). The *k*-distance of a sample describes its local density: The more the *k*-distance, the less the local density. It follows that the weight of a neighboring sample depends on the density of this sample. For a normal sample, its neighboring samples are mostly normal, and its weighted neighborhood density is similar to its average neighborhood density. But for an anomaly, the proportion of anomalies in its neighborhood is uncertain when the parameter *k* is small. When a large proportion of samples are anomalies in the neighborhood of an anomaly, the average neighborhood density may be drastically decreased, which influences the detection of the anomaly. However, the weighted neighborhood density of an anomaly is obviously larger than the average neighborhood density. Then, the anomaly is easier to detect using the weighted neighborhood density. Therefore, the range of appropriate values of *k* for the weighted neighborhood density estimation is much wider than the range for the traditional average neighborhood density estimation. This means that our weighted neighborhood density estimation is more robust to the variations in the value of *k*. Our weighted neighborhood density estimation can replace the average neighborhood density estimation in any local density-based anomaly detection method, and make the method less sensitive to the parameter *k*.

2.5. Anomaly factor estimation

The anomaly factor is used to estimate the extent to which a sample is an anomaly. Normal samples lie in dense regions, and then they have high local densities and close neighborhood densities. Anomalies lie in sparse regions and have low local densities. The local kernel density and weighted neighborhood density-based anomaly factor $WAF(\mathbf{p})$ of a sample **p** is defined as:

$$WAF(\mathbf{p}) = \frac{wde(\mathbf{p})}{kde(\mathbf{p})} \tag{12}$$

The less a sample’s local kernel density and the larger the weighted density of its neighborhood, the larger the anomaly factor and the more probably the sample is an anomaly. For most anomalies which are isolated from the cluster, their local densities are much different from their neighborhood densities, ensuring that their anomaly factors are much larger than 1. For most samples in a cluster, their local densities are closer to their neighborhood densities, ensuring that their anomaly factors fluctuate around 1. This makes it easy to distinguish between anomalies and normal samples.

Given the anomaly factors of all the samples, the anomalies are detected in the following ways:

- The top *N* samples listed in the descending order of anomaly factors are considered as anomalies.
- The samples whose anomaly factors are larger than a threshold are considered as anomalies.

Appendix B gives a mathematical proof of the claim that the weighted neighborhood density estimation is more robust to the parameter *k* than the traditional average neighborhood density estimation for anomaly factor estimation. This gives a theoretical support to the robustness of our anomaly detection method to the neighborhood size parameter.

2.6. Computational complexity

Computation of the anomaly factors based on local kernel density and weighted neighborhood density includes the following two steps:

- The *k*-distance neighbors for each sample are found.
- The whole dataset is traversed, and the $kde(\mathbf{p})$, $wde(\mathbf{p})$, and $WAF(\mathbf{p})$ values for each sample **p** are computed.

Without optimization, the computational complexity of the first step is $O(n^2)$ where *n* is the number of samples in the dataset. By optimization using an index technology, such as the K-D index tree algorithm [7, 20], the computational complexity is reduced to $O(n\log n)$. The computational complexity of the second step is $O(nk)$, since both $kde(\mathbf{p})$ and $wde(\mathbf{p})$ are computed in the *k*-distance neighborhood of **p**. Hence, the total computational complexity of our local kernel and weighted neighborhood density-based anomaly detection method is $O(n\,log\,n+nk)$. The larger the *k* is, the more the runtime. Increasing the robustness to the parameter *k* not only overcomes the difficulty in determining the value of *k* without any prior knowledge, but also ensures that a lower value of *k* can be used thus reducing the runtime.

2.7. Limitations

There are the following two limitations in the local kernel density-based local anomaly factor estimation method:

- Anomaly factors are not accurate enough to rank all the samples in the database. In the local density-based methods, the anomaly factor of a sample is determined by both the estimate of its density and the density estimate of its neighborhood. As shown in Fig. 6, sample A is close to cluster D_2 and sample B is close to cluster D_1. Cluster D_1 has a larger density than cluster D_2. Then, the estimated anomaly factor of sample A is smaller than that of sample B. However, as sample A is farther away from the normal sample clusters, it has a higher probability of being an anomaly than sample B in practice.
- The local kernel-based local anomaly factor of a sample depends on the density estimation in its neighborhood. The estimated local anomaly factors in the same cluster may differ widely because of different neighborhood densities. With a fixed value of *k* for all the samples, the neighborhood density estimation may not be accurate enough to express the relative magnitudes of the neighborhood densities of different samples. If the anomalies are randomly distributed in a number of clusters that have different densities, a single value of *k* may not be appropriate for detecting all the anomalies. Then, the estimated local anomaly factor values are not accurate enough to rank all the samples in a complex database with highly variable region densities.

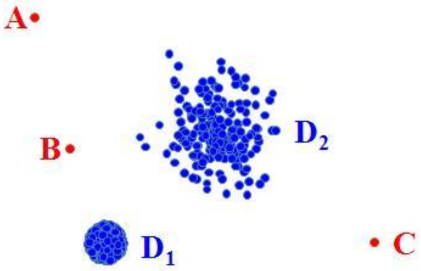

Fig. 6. The inaccurate anomaly factors for local density-based methods.

3. Hierarchical Context-Based Kernel Regression

In order to handle the above limitations of local density-based methods, we propose to adopt non-parametric regression to refine the anomaly factors obtained by a local density-based method $F()$. The dataset $\{\mathbf{x}_1,\mathbf{x}_2,...,\mathbf{x}_n\}$ is preprocessed:

$$\{\mathbf{x}_1,...,\mathbf{x}_n\} \overset{F(\mathbf{x})}{\Rightarrow} \{(y_1,\mathbf{x}_1),...,(y_n,\mathbf{x}_n)\} \tag{13}$$

where y_i is sample $\mathbf{x}_i$'s anomaly factor estimated by $F(\mathbf{x})$. We propose a multi-scale local kernel regression method to combine the information from multiple scale neighborhoods to hierarchically refine the anomaly factors $\{y_1,y_2,...,y_n\}$.

3.1. Local kernel regression

Nadaraya-Watson kernel regression is a classic nonparametric regression method [21]. It has strong adaptability, high robustness, and unfettered regression function forms. It is able to effectively handle nonlinear inhomogeneous regression problems.

Given a dataset $\{(y_1, \mathbf{x}_1), (y_2, \mathbf{x}_2), ..., (y_n, \mathbf{x}_n)\}$, the Nadaraya-Watson kernel regression estimates the dependent parameter *y* of a vector **x** in the following way:

$$y = \frac{\sum_{i=1}^{n} \frac{1}{(\lambda_i)^{\gamma}} K\left(\frac{\mathbf{x}-\mathbf{x}_i}{\lambda_i}\right) y_i}{\sum_{i=1}^{n} \frac{1}{(\lambda_i)^{\gamma}} K\left(\frac{\mathbf{x}-\mathbf{x}_i}{\lambda_i}\right)} \tag{14}$$

where λ_i is an adaptive smoothing parameter, γ is a sensitivity parameter, and $K()$ is a multivariate kernel function. The Nadaraya-Watson kernel regression attains the estimation of *y* for sample **x** using the weighted average of $\{y_1, ..., y_n\}$. The weight depends on:

- the kernel function *K*() which determines the mapping relation between the weight of $\mathbf{x}_i$ and the difference between **x** and $\mathbf{x}_i$.
- the parameter λ_i which determines the size of the window of the kernel function.

Intuitively, the less the difference between **x** and **x**$_i$, the larger the weight for $\mathbf{x}_i$, and the closer the value *y* is to y_i. The Nadaraya-Watson kernel regression estimator avoids the parameter solving process in the traditional linear regression models. It is more adaptable to complex samples which are nonlinearly distributed. The limitation of the Nadaraya-Watson regression is that it is necessary to traverse all the samples in the dataset **to estimate** the regression value of a new sample, and then the computational complexity is high.

To reduce the computational complexity of the Nadaraya-Watson regression, we extend it to propose a local kernel regression estimator which is computed locally in the *k*-distance neighborhood of a sample. The local kernel regression estimator of a sample **p** is defined as:

$$y_{\mathbf{p}} = \frac{\sum_{\mathbf{q} \in N_k(\mathbf{p})} \frac{1}{\left(d_k(\mathbf{q})\right)^{\gamma}} K\left(\frac{\mathbf{p}-\mathbf{q}}{d_k(\mathbf{q})}\right) y_{\mathbf{q}}}{\sum_{\mathbf{q} \in N_k(\mathbf{p})} \frac{1}{\left(d_k(\mathbf{q})\right)^{\gamma}} K\left(\frac{\mathbf{p}-\mathbf{q}}{d_k(\mathbf{q})}\right)} \tag{15}$$

where sample **q** is a *k*-distance neighbor of **p** and $y_{\mathbf{q}}$ is the anomaly factor of **q**. The local kernel regression estimator is different from the Nadaraya-Watson kernel regression in the following ways:

- The computational complexity of the Nadaraya-Watson regression for estimating the dependent parameter of a sample is *O*(*n*). The computational complexity of our local regression estimator for a sample is *O*(*k*). It is apparent that *k*<<*n*. Our local regression estimator has a much lower computational complexity than the

Nadaraya-Watson regression estimator.

- In the Nadaraya-Watson regression, the parameter γ is usually set to the dimension *d* of the sample vectors. In high dimensional databases, (*k*-distance)^d is unstable, because when *k*-distance is small (*k*-distance)^d approximates to 0, and when *k*-distance is large (*k*-distance)^d is very large. This makes the regression estimator indiscriminative to samples. To obtain a balance between the sensitivity and the robustness, a default value of γ is 2, which is verified as an optimal value by our experiments.
- The window control parameter λ_i for a sample *i* in the Nadaraya-Watson regression becomes the *k*-distance of the sample in our local kernel regression estimator. We use the *k* distance of each sample in the neighborhood to control the size of the window. This ensures that the size of the window is adaptively adjusted in a data-driven way. Selection of the parameter λ for a sample as in the Nadaraya-Watson regression is avoided.

3.2. Context-based kernel

The kernel *K*() in (15) is critical for determining the performance of the local kernel regression. The kernel function in the local regression has the following requirements:

- It should effectively keep high anomaly factors for the isolated anomalies which can be easily detected by the local anomaly detection methods, such as our method based on local kernel and weighted neighborhood density.
- It should make the anomaly factors of anomalies in the same cluster close to each other and obviously distinguishable from the factors of normal samples.

The local kernel function should be able to utilize the relation between a sample and its *k*-distance neighbors, besides only using the differences between samples and the neighborhood size to determine the weight of each neighbor.

The traditional kernels, such as the Gaussian kernel and the Epanechnikov kernel, cannot meet the above requirements. So, we propose a new kernel function which is defined as follows for a variable vector **z**:

$$K(\mathbf{z}) = \begin{cases} \beta, & if\ \|\mathbf{z}\| \le 1 \\ \beta \exp\left(-\frac{(\|\mathbf{z}\|-1)^2}{2}\right), & otherwise \end{cases} \tag{16}$$

where the constant β is chosen to ensure that $K()$ integrates to 1 (The mathematical derivation of β is included in Appendix A). Based on the new kernel, the local kernel regression estimator computes the weight of a *k*-distance neighbor **q** of a sample **p** according to the followed rules:

- If **p** is also a *k*-distance neighbor of **q**, then $\|\mathbf{p}-\mathbf{q}\| \le d_k(\mathbf{q})$ and

$$K\left(\frac{\mathbf{p}-\mathbf{q}}{d_k(\mathbf{q})}\right) = \beta . \tag{17}$$

- If **p** is not a *k*-distance neighbor of **q**, then $\|\mathbf{p}-\mathbf{q}\| > d_k(\mathbf{q})$, and

$$K\left(\frac{\mathbf{p}-\mathbf{q})}{d_k(\mathbf{q})}\right) = \beta \exp\left(-\frac{\left(\frac{\|\mathbf{p}-\mathbf{q}\|}{d_k(\mathbf{q})}-1\right)^2}{2}\right). \tag{18}$$

  The kernel value of **q** is, with the maximum *β*, a monotonically decreasing function of the difference between **p** and **q**.

The reason for the first rule is that, if either of two samples is a neighbor of the other sample, then they have similar local distributions and they are likely to belong to the same cluster. Therefore, both of them are assigned larger weights to obtain similar anomaly factors. The reason for the second rule is that, if only one of two samples is a neighbor of the other sample, then they are less closely related, and thus we use their difference to inversely weight them. In this way, our neighborhood context-based kernel retains the properties of the traditional kernels. It also considers the different properties of isolated anomalies and anomalies distributed in clusters and deals with these two types of anomalies differently. By combining similarities between samples and the neighborhood context, our kernel can more effectively distinguish anomalies from normal samples.

3.3. Hierarchical kernel regression

A complex dataset includes anomalies which are easier to detect by taking into account the global distribution of all the samples and anomalies which are distributed in small clusters and are easier to detect locally. We propose a hierarchical kernel regression strategy which iteratively updates anomaly factors of samples using our local kernel regression method by gradually enlarging the size of the neighborhood. In this way, sample anomaly factors are estimated both locally and globally to increase their accuracies.

The hierarchical kernel regression-based anomaly detection method initializes the anomaly factors $\{y_1^0,...,y_n^0\}$ for the samples using the anomaly factors obtained by the local kernel density and weighted neighborhood density-based method described in Section 2. The initial value k_0 of *k* for the hierarchical updating process is set to the value of *k* used in the initial anomaly factor estimation. Isolated anomalies should be specifically handled to avoid that the anomaly factor of an isolated anomaly is smoothed by its *k*-neighbors. As shown in Fig. 6, isolated samples are obviously far from other samples. We propose to use the neighborhood context to identify isolated anomalies, i.e., if a sample is not a *k*-neighbor of its own *k*-neighbors, then there is no similar sample in its neighborhood and the sample is treated as an isolated sample. The anomaly factors of isolated anomalies are kept unchanged, because the anomaly factors of the isolated anomalies usually have been accurately estimated by the initial local density-based method. In this way, our regression method effectively handles the isolated anomalies and increases the accuracy of detecting anomalies distributed in clusters. Our hierarchical kernel regression-based anomaly detection process is outlined as follows:

Step 1: $1 \rightarrow t$; $k_0 \rightarrow k$; $\{y_1^0,...,y_n^0\}$ is given.

Step 2: Determine the *k*-distance neighborhoods for all the samples.

Step 3: Compute $\{y_1^t,...,y_n^t\}$ using the local kernel regression estimator (15), given $\{y_1^{t-1},...,y_n^{t-1}\}$;

If $\forall \mathbf{q} \in N_k(\mathbf{p})$ $\|\mathbf{p}-\mathbf{q}\| > d_k(\mathbf{q})$, then **p** is identified as an isolated anomaly and $y_{\mathbf{p}}^t = y_{\mathbf{p}}^{t-1}$.

Step 4: If $\sum_{i=1}^{n} | y_i^t - y_i^{t-1} |$ is less than a threshold or a predefined number of iterations is reached, then go to Step 5; otherwise $t+1 \rightarrow t$, $k + \Delta \rightarrow k$ (Δ is a stepping factor), and go to Step 2 for another loop of iteration.

Step 5: Output the anomaly factors $\{y_1^t,...,y_n^t\}$.

Our hierarchical kernel regression combines the multiple scale information from the different sizes of neighborhoods using the local kernel regression estimator. This combination makes the hierarchical kernel regression more effective in detecting anomalies in mixed and large databases.

4. Spatial Constrained Anomaly Detection: Image Saliency Detection

We apply the above general anomaly detection theory to image saliency detection [47, 48], and propose a spatial constrained anomaly detection method. Salient regions in an image deviate from the background regions and capture the attention of human viewers. This makes it possible to treat salient pixels in object regions as anomalies and background regions as normal, and then use our unsupervised anomaly detection method to construct a saliency map. In contrast to pure anomaly detection, saliency detection combines visual feature contrast information and pixels' spatial distribution information. A saliency detection method is proposed, which consists of local density-based saliency map computation in the feature space and saliency score propagation in the image.

4.1. Local density-based saliency map

According to the human vision attention mechanism theory, the saliency of a pixel depends on its appearance and its context with its surrounding pixels. Hence, we use visual features of the image patch centered at each pixel, instead of only the pixel value itself. Let $\mathbf{c}_j$ be the value vector of pixel *j* in the CIE L*a*b* color space. A pixel *i* is represented by a visual feature vector $\mathbf{v}_i$ describing the image patch I_i centered at pixel *i*:

$$\mathbf{v}_i = \frac{\sum_{j \in I_i} \omega_j \mathbf{c}_j}{\sum_{j \in I_i} \omega_j} \tag{19}$$

where ω_j is the weight for pixel *j*. The weight is computed by:

$$\omega_j = \frac{1}{\sqrt{2\pi}} \exp\left(-\frac{d_{spatial}(i,j)^2}{2} \right) \tag{20}$$

where $d_{spatial}(i, j)$ is the Euclidean distance between the positions of pixels *i* and *j*. A pixel *i* is considered as salient if the appearance of its patch I_i deviates from the majority of patches in the visual feature space. Given the visual feature vector set $\{\mathbf{v}_i\}$ of all the patches in an image, we propose to estimate the saliency score $S(i)$ for each pixel *i* using anomaly factor obtained by comparing the local density of the patch I_i with its neighborhood density using the anomaly detection method in Section 2.

We use local density estimations from multi-scales which are obtained by shrinking (subsampling) the original image, to improve the saliency scores. As a prior knowledge, background patches always have more similar appearances than salient patches. This indicates that a background patch and its *k*-nearest neighbors in the visual feature space follow the more similar distributions than a salient patch in multi-scales. For each shrunken image, we estimate its saliency map and then enlarge the saliency map to the same size as the original image. In this way, a number of saliency scores for each pixel in multiple scales are obtained. To improve the visual contrast between salient patches and background patches, we combine these saliency scores by:

$$S(i) \leftarrow \frac{1}{|L|}\sum_{l\in L} S_l(i) \tag{21}$$

where $S_l(i)$ is the saliency score of pixel *i* in a scale *l*, and *L* is the multi-scale set with the size of $|L|$.

4.2. Kernel-based saliency score propagation

The above local density-based saliency map computation captures the salient pixels which are the foci of human attention. We keep the original saliency scores of the pixels which have large saliency scores, and propose a kernel-based saliency score propagation method to adjust the saliency scores of other pixels. This propagation method which is similar to the local kernel regression in Section 3.1 is defined as follows:

$$\bar{S}(i) = \frac{\sum_{j\in\{N^k_{Spatical}(i),i\}} K\left(\frac{\mathbf{v}_i-\mathbf{v}_j}{d_k(\mathbf{v}_j)}\right)S(j)}{\sum_{j\in\{N^k_{Spatical}(i),i\}} K\left(\frac{\mathbf{v}_i-\mathbf{v}_j}{d_k(\mathbf{v}_j)}\right)} \tag{22}$$

where *K*() is a kernel function as defined in (16), and different from (15) the neighborhood $N^k_{Spatial}(i)$ is defined in the image space rather than in the visual feature space. Our kernel-based saliency score propagation method causes that pixels in the same salient region achieve closer saliency scores. According to the definition of *K*(), if either of patch *i* and one of its spatial neighbors lies in the *k*-nearest neighborhood of the other patch in the feature space, the weight of the spatial neighbor patch is set to be the maximum. Our saliency score propagation method ensures that **pixels** spatially near to the pixels which have large saliency scores increase their saliency scores, while the background pixels have low saliency scores.

5. Experiments

We evaluated the anomaly detection capability of the proposed methods by comparison with the state-of-the-art methods on several synthetic and real datasets. We compared our image saliency detection method with the state-of-the-art methods on a publicly available dataset. In the experiments, there are a few parameters and thresholds which were determined by cross-validation. The parameter γ in (3) was set to 2. The parameters α and C in (5) were set to 1. The parameter σ in (10) was set to 1 except for testing the effect of σ. The parameter γ in (15) was set to 2. The initial value k_0 of k for the hierarchical context-based kernel regression updating process was set to 1.5% of the number of samples in the dataset. The stepping factor Δ was set to 2.5% of the number of samples in the dataset. The maximum number of iterations was set to 5. For image saliency detection, each pixel was expressed by a patch of size of 7*7 pixels. Saliency scores in (21) were computed in the four scales which correspond to the sizes of 100%, 50%, 25%, and 12.5% of the original image. The neighborhood size in the image space in (22) was set to 10% of the number of pixels in the image.

In the following, we first evaluated the robustness of our local kernel and weighted neighborhood density-based method to the neighborhood parameter k on two synthetic datasets. Then, we compared our local kernel and weighted neighborhood density-based anomaly detection method and the hierarchical local regression-based method with several state-of-the-art anomaly detection methods on several real datasets. Finally, the comparison results for image saliency detection were reported.

5.1. Synthetic datasets

Fig. 7 shows two synthetic datasets. The Synthetic-1 dataset consists of 1500 normal samples and 16 anomalies. The normal samples are distributed in three clusters where each cluster contains 500 normal samples. Fifteen anomalies lie in a cluster whose center is equidistant from the centers of the three clusters of the normal samples; and one anomaly is isolated from all the others. The Synthetic-2 dataset consists of 1000 normal samples and 20 anomalies. There are 500 normal samples uniformly distributed in an annular region and 500 normal samples distributed in a cluster. There are 10 anomalies lying in the center of the annular region and 10 anomalies distributed between the two clusters of the normal samples.

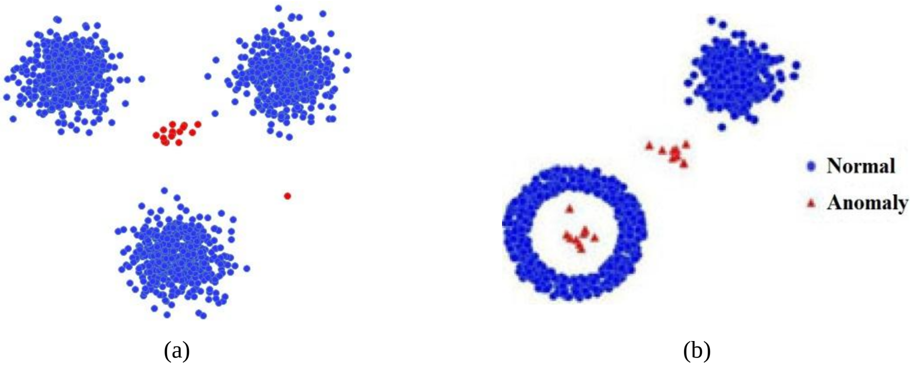

(a) (b)

Fig. 7. The distributions of two synthetic datasets: (a) Synthetic dataset 1; (b) Synthetic dataset 2.

We compared our local kernel and weighted neighborhood density-based method with the baseline [7] of our work. In the baseline [7], the local anomaly factor of a sample is the ratio of its neighborhood density to its own density. Table 2 shows the anomaly detection results of the baseline [7] and our method on the Synthetic-1 dataset, when the weight parameter σ in (10) was set to 0.1 and 1. The performance of anomaly detection was estimated using the number and proportion of the anomalies in the 16 samples which have the largest estimated anomaly factors. It is seen that our local kernel and weighted neighborhood density-based method identifies all the anomalies when $k \geq 27$ and σ = 0.1 and detects all the anomalies when $k \geq 31$ and σ = 1. The baseline is unable to identify all the anomalies until $k = 60$. This indicates the following points:

- The available range of *k* for our method is much larger than the range for the baseline. So, our method is less sensitive to the parameter k .
- The value of *k* for our method to reach the best performance is much smaller than that for the baseline, so our method can obtain the same result as the baseline with less runtime.
- Our method is robust to the parameter σ .

Table 2. Results of anomaly detection on the Synthetic-1 dataset: the number and proportion of anomalies in the top-16 samples

k	Baseline [7]	Our local kernel method	
		σ = 0.1	σ = 1
26	1(6.25%)	15(93.75%)	15(93.75%)
27	2(12.5%)	16(100%)	15(93.75%)
30	4(25%)	16(100%)	15(93.75%)
31	5(31.25%)	16(100%)	16(100%)
59	15(93.75%)	16(100%)	16(100%)
60	16(100%)	16(100%)	16(100%)
70	16(100%)	16(100%)	16(100%)

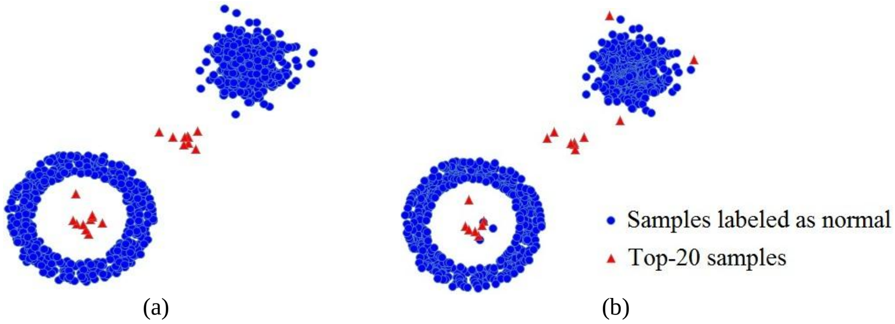

Fig. 8. The best results of our method and the baseline on the Synthetic-2 dataset: (a) The results of our local kernel and the weighted neighborhood density-based method with *k*=14; (b) The results of the baseline [7] with *k*=20.

Fig. 8 shows the best results that our method and the baseline obtain on the Synthetic-2 dataset. It seen that our method captures all the anomalies in the top-20 sample list of anomaly factors when *k*=14. The baseline obtains its best performance when *k*=20, and only 17 anomalies are correctly detected in its top-20 sample list. Compared with our method, the baseline cannot detect all the anomalies whatever the value of *k*, because the annular cluster distribution in the samples poses an obstacle for the baseline method to detect anomalies. The results indicate that our method is more adaptable to the complex datasets than the baseline.

5.2. Real datasets

The following public real datasets were used to compare our methods with the state-of-the-art anomaly detection methods:

- **The KDD Cup 1999:** This is a general dataset for network intrusion detection research. The 60593 normal sample and the 228 U2R attack samples labeled as anomalies were selected to form the KDD dataset for anomaly detection. Each sample is described by 41 features.
- **The Mammography dataset:** This dataset was extracted from a mammography image dataset. It includes 10923 normal samples and 260 anomalies. Each sample consists of 6 features.
- **The Ann-thyroid dataset:** This is a dataset of pathological thyroid changes. It consists of 73 anomalies and 3178 normal samples. Each sample consists of 21 features.
- **The Shuttle dataset:** This dataset has six classes in which there are 11478, 13, 39, 809, 4, and 2 samples, respectively. Five test datasets were constructed. The samples in the largest class become the normal samples in all the five test datasets. The samples in one of the other five classes become anomalies in a test dataset. Each sample is described by a 9-dimensional feature vector.
- **The visual trajectory dataset:** The trajectories in this dataset were captured by tracking vehicles in a crowded traffic scene. There are 1500 normal trajectories and 50 anomalies which correspond to traffic offences or tracking errors. Each trajectory was linearly interpolated with points to ensure that all the trajectories have the same number of points. The coordinates of the points in a trajectory form a vector representing the trajectory.

The samples in these datasets were preprocessed by the inverse document frequency method [10, 13, 14] in order that the discrete features can be handled in the same way as the continuous features.

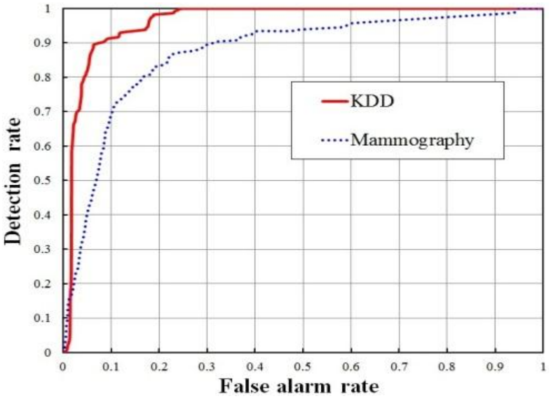

Fig. 9. ROC curves of our local kernel and weighted neighborhood density-based method on the KDD and the Mammography datasets.

For the real datasets, the performance of anomaly detection was evaluated using the values of areas under the curves (AUC) of the receiver operating characteristic (ROC). A ROC curve was drawn by using the detection rate as the y-coordinate and the false alarm rate as the x-coordinate. As an example, Fig. 9 shows the ROC curves of our local kernel and weighted neighborhood density-based method on the KDD dataset and the Mammography dataset. The AUC value is the surface area under the ROC curve. The larger the AUC value, the more accurate the anomaly detection result. The AUC value on the Shuttle dataset is the average AUC of all the five subsets.

Table 3. The AUC values of our local kernel and weighted neighborhood density-based method with different kernels on the real datasets

Datasets Kernels	KDD	Mammography	Ann-thyroid	Shuttle (average)	Trajectory
Our kernel	0.962	0.871	0.970	0.990	0.979
Gaussian kernel	0.961	0.870	0.970	0.990	0.976
Epanechnikov kernel	0.944	0.855	0.965	0.993	0.973

Table 4. The runtimes (seconds) of our local kernel and weighted neighborhood density-based method with different kernels on the real datasets

Datasets Kernels	KDD	Mammography	Ann-thyroid	Shuttle (average)	Trajectory
Our kernel	1918.1	15.8	4.9	36.4	4.1
Gaussian kernel	2095.2	19.8	5.2	36.9	5.5
Epanechnikov kernel	2363.7	48.2	13.2	66.7	12.3

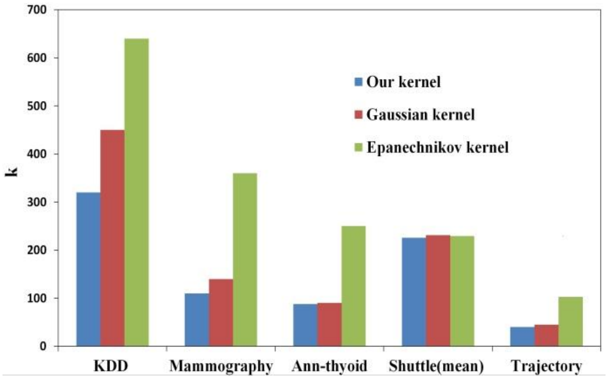

Fig. 10. The values of *k* with the best results for different kernels.

We compared the performances of our local kernel and weighted neighborhood density-based method when the Gaussian kernel, the Epanechnikov kernel, and our Volcano kernel were used respectively, where the parameters and thresholds were kept unchanged. Tables 3 and 4 show, respectively, the AUC values and the runtimes of our local kernel and weighted neighborhood density-based method with different kernels on the real datasets. Fig. 10 shows the values of *k* for all the three kernels on all the datasets when the best detection results were obtained. It is seen that although the detection accuracy of our Volcano kernel is overall only slightly higher that the detection accuracy of the Gaussian kernel and the Epanechnikov kernel, the neighborhood size *k* with the best results for our Volcano kernel are smaller than those of the other kernels. This supports the claim that our kernel achieves the least runtime. The reason is that for our Volcano kernel only a line segment is used to represent the densities when $\|\mathbf{z}\|$ is within [-1,1], while a curve segment is used for the Gaussian kernel or the Epanechnikov kernel. Estimation of the density of a normal sample using the Volcano kernel requires fewer neighboring samples than estimation using the Gaussian kernel or the Epanechnikov kernel (See Section 2.3).

We compared our method with the following eight state-of-the-art anomaly detection methods:

- The local anomaly factor-based method [7] (the baseline of our work): The local outlier factor captures the relative degree to which the sample is isolated from its surrounding neighborhood.
- The local density factor-based method [9]: This method modifies a nonparametric density estimate with a variable kernel to yield local density estimation. Anomalies are then detected by comparing the local density of each sample to the local density of its neighbors.
- The local peculiarity factor-based method in [10]: This method applies the local peculiarity factor which is the μ-sensitive peculiarity description for general distributions to anomaly detection.
- The feature bagging-based method [13]: This method combines anomaly scores computed by the individual anomaly detection algorithms that are applied using different sets of features to more accurately detect anomalies.
- The active learning-based method [14]: This method detects anomalies by classifying a labeled data set containing artificially generated anomalies. Then, a selective sampling mechanism based on active learning was invoked for the reduced classification problem.
- The bagging-based method in [14, 15]: The bagging method in [15] was applied to detect anomalies using the same component algorithm in [14] on the same reduced problem in [14].
- The boosting-based method in [14, 16]: The boosting-based method was applied to detect anomalies using the same component algorithm in [14] on the same reduced problem in [14].
- The generalized density-based anomaly detection method in [56]: This method produces a series of density estimates. The *z*-score transformation was applied to standardize the deviation from normal density. A rescaling was applied to obtain the anomaly score.

Table 5 shows the AUC values of our method and the competing methods on the real datasets. The AUC values of the competing methods, except for the generalized density-based anomaly detection method [56], on the KDD, Mammography, Ann-thyroid, and Shuttle datasets were directly taken from the publications [7, 9, 10, 13, 14, 15, 16]. The setting of the parameters in these competing methods can be found in the publications. For the generalized density-based anomaly detection method, the setting of the minimum and maximum values of k is the same as for our hierarchical context-based kernel regression method. Other parameters were tuned to make the results as accurate as possible. Table 6 shows the runtimes of the local density-based methods. Since the local peculiarity factor-based method has the much higher complexity and needs much more runtime than other methods, its accurate runtime was not given. The runtimes for the other competing methods are not available in the literature. Fig. 11 shows the AUC values of our local kernel and weighted neighborhood density-based method with different values of *k* on the KDD and Mammography datasets which are the largest datasets in all the datasets. From these tables and figures, the following points are revealed:

Table 5. The AUC values of our method based on local kernel and weighted neighborhood density and the competing methods on the real datasets.

Datasets Methods	KDD	Mammography	Ann-thyroid	Shuttle (average)	Trajectory
Our local kernel method	0.962	0.871	0.970	0.990	0.961
Local anomaly factor [7]	0.610	0.640	0.869	0.852	0.835
Local density factor [9]	0.941	0.824	0.943	0.962	0.856
Density-based anomaly [56]	0.97	0.870	0.970	0.988	0.936
Local peculiarity factor [10]	0.98	0.87	0.97	0.992	0.868
Bagging [15]	0.61	0.74	0.98	0.985	--
Boosting [16]	0.51	0.56	0.64	0.784	--
Feature bagging [13]	0.74	0.80	0.869	0.839	--
Active learning [14]	0.94	0.81	0.970	0.999	0.836

Table 6. The runtimes (seconds) of our method based on local kernel and weighted neighborhood density and the competing methods on the real datasets.

Datasets Methods	KDD	Mammography	Ann-thyroid	Shuttle	Trajectory
Our local kernel method	1918.1	15.8	4.9	36.4	3.5
local anomaly factor [7]	2160.1	28.8	5.9	42.0	4.5
Local density factor [9]	2214.9	36.4	7.2	37.1	5.1
Density-based anomaly [56]	2791.5	45.3	8.1	53.8	5.6
Local peculiarity factor [10]	>>2214.9	>>36.4	>>7.2	>>37.1	>>5.1

- Overall, our local kernel and weighted neighborhood density-based method always achieves the best performance or close to the best performance in all the datasets. No method is the winner on all the datasets.
- On all the datasets, our local kernel and weighted neighborhood density-based method has less runtime than the competing local density-based methods: the local anomaly factor-based method, the local density factor-based method [9], the local peculiarity factor-based method**,** and the generalized density-based method [56]. The generalized density-based method [56] yields much more accurate results than the local anomaly factor method [7] and the local density factor method [9]. The runtimes of the generalized density-based method [56] are comparable to those of the local anomaly factor method [7] and the local density factor method [9].
- The AUC values of our local kernel and weighted neighborhood density-based method on the KDD dataset are larger than 0.941, when *k* varies from 280 to 700. The AUC values of our method on the Mammography dataset are larger than 0.824, when *k* varies from 40 to 460. These detection accuracies are higher than those of the other competing methods except for the local peculiarity factor-based method and the generalized density-based method.
- On the Mammography dataset, our local kernel-based method yielded a more accurate result than the competing methods when *k*=110, and a comparable result was obtained by the local peculiarity factor-based

method when *k*=11183. On the KDD dataset, our local kernel-based method yielded an accurate result when *k*=320, and the most accurate result was obtained by the local peculiarity factor-based method when *k*=13000. The complexity of the local peculiarity factor-based method is $O(nd\log(n)+ndk)$ while the complexity of our local kernel-based method is $O(n\log(n)+nk)$. It is apparent that the local peculiarity factor-based method needs much more runtime than our local kernel-based method.

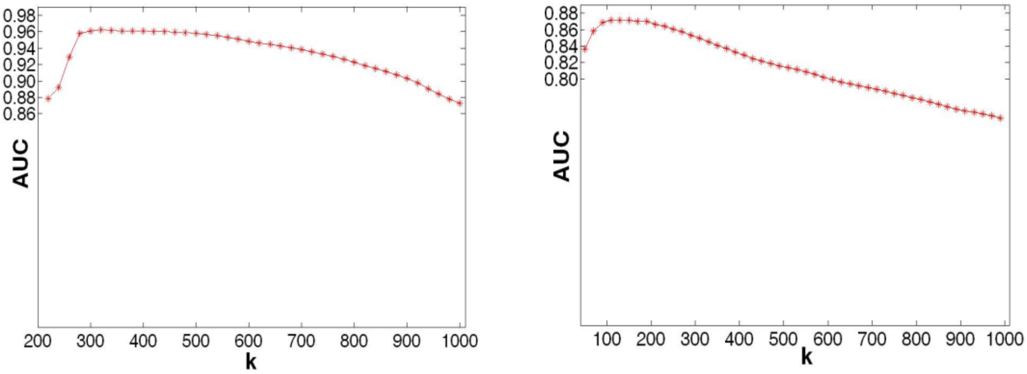

(a)

(b)

Fig. 11. The AUC values of our local kernel and weighted neighborhood density-based method with different k values on (a) the KDD dataset and (b) the Mammography dataset.

Table 7 shows the AUC values obtained after refining the results of the local anomaly factor method and the results of our local kernel and weighted neighborhood density-based method using our hierarchical context-based kernel regression method in Section 3. From Tables 5 and 7, it is seen that our hierarchical kernel regression method greatly improves the results of the local anomaly factor-based method. The AUC values obtained by refining the results of our local kernel and weighted neighborhood density-based method are larger than the values obtained by refining the results of the local anomaly factor-based method. The multiple scale combination together with the local density anomaly factor estimation effectively captures both the global and local properties of samples, and is then more effective for the mixed large databases.

Table 7. The AUC values of our hierarchical context-based kernel regression method on the real datasets.

Datasets Initialization	KDD	Mammography	Ann-thyroid	Shuttle	Trajectory
Local anomaly factor [7]	0.983	0.871	0.975	0.992	0.971
Our local kernel method	0.990	0.879	0.982	0.998	0.986

We analyze the result differences between different datasets from different types of applications as follows:

- On the KDD dataset, anomaly detection methods obtain comparatively accurate results. This is because the network attacks are easily distinguishable from normal network links corresponding to normal samples and the ratio of anomalies in the dataset is very small.
- On the Mammography dataset, lower detection accuracies are obtained by anomaly detection methods. The mammography images with cancers are less distinguishable from images without cancers.

- In contrast with mammography images, samples with thyroid pathological changes are more readily distinguished from normal thyroid samples. The detection accuracy on the Ann-thyroid dataset is higher than that on the Mammography dataset.
- On the Shuttle dataset, the final accuracy is the average of five test datasets. In four of the five test datasets a very small portion of samples are anomalies. This makes these anomalies very easy to identify and substantially increases the average accuracy on the five test datasets.
- On the KDD dataset, the Mammography dataset, the Ann-thyroid, and the Shuttle dataset, the supplied data are feature vectors extracted from samples. On the visual trajectory dataset, the coordinates of the points in a linearly interpolated trajectory form a feature vector which was used as the input to the anomaly detection methods. Extracting feature vectors in this way keeps the spatial information on trajectories but loses their temporal information. This partly causes failures in detecting abnormal trajectories.

5.3. Image saliency detection

In the application of image salience detection, feature vectors of the image patch centered at each pixel were used as the data for the anomaly detection methods. Spatial information in images was used to propagate saliency scores of pixels.

We compared our anomaly detection-based saliency detection method with the following state-of-art methods: Itti's method [42], Hou's method [43], Seo's method [44], the graph-based method in [45], and the frequency tuned method in [46] on a publicly available dataset. The results of the competing methods were taken from the publications [42, 43, 44, 45, 46]. The setting of the parameters in these competing methods can be found in the publications. This dataset is the Microsoft visual salient image set which contains 5000 high quality images. For each image in the set, 9 users were requested to draw a bounding box around the most salient region. All the users' annotations were averaged to create a saliency map for the image. However, the bounding box-based ground truth is not accurate. Achanta et al. [46] chose 1000 images from the original set and constructed an object-contour based ground truth for them. The corresponding binary saliency maps were also given.

All the saliency detection methods were evaluated using Precision, Recall, and F measure. Let $S_{truth}(i)$ be the true binary saliency score for pixel i, and $S(i)$ be the binary saliency score for pixel i computed by the saliency detection method. The three measures are formulated as:

$$Precision = \frac{\sum_i S_{truth}(i)S(i)}{\sum_i S(i)} \tag{23}$$

$$Recall = \frac{\sum_i S_{truth}(i)S(i)}{\sum_i S_{truth}(i)} \tag{24}$$

$$F_{score} = \frac{(1+\eta)Precison * Recall}{\eta Precision + Recall} \tag{25}$$

where parameter η was set to 0.5 to balance the precision and the recall.

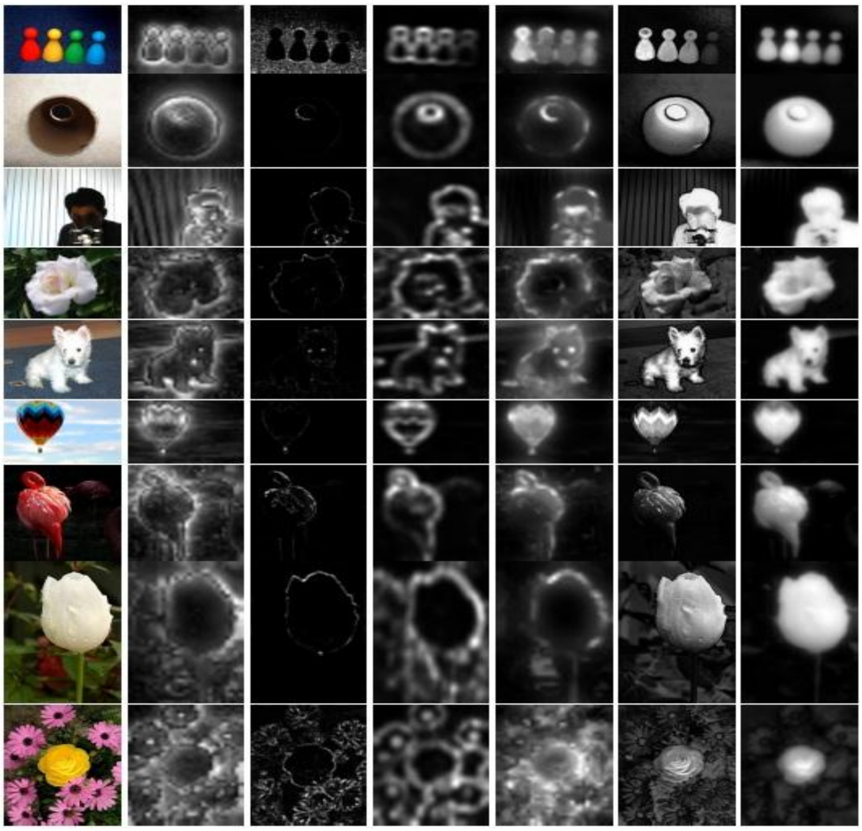

Fig. 12. Visual comparison of saliency maps: (a) Original images; (b) Itti's method [42]; (c) Hou's method [43]; (d) Seo's method [44]; (e) The graph-based method [45]; (f) The frequency tuned method [46]; (g) Our method.

To use the precision, recall and F measure, the original saliency scores were transformed to a binary saliency map using a threshold *T*, i.e., pixels that have saliency scores above the threshold *T* are identified as salient. Achanta et al. [46] set the threshold of an image to be twice the mean of the saliency scores of the pixels in the entire image. This method does not consider the information in the distribution of the saliency scores. We propose to combine the standard deviation and mean of saliency scores in an image to determine the threshold. Let *Std* and *Mean* be, respectively, the standard deviation and mean of saliency scores in an image. Our method is formulated as:

$$T = \mu * Std + Mean \tag{26}$$

where parameter μ was set to 0.1 in the experiments. If saliency scores follow a Gaussian distribution, this value of μ indicates that more than 15% of pixels are treated as salient. We used both Achanta's method and our method to produce binary saliency maps, and measure the performances of the saliency detection methods.

Fig. 12 shows some examples of saliency maps obtained by our method and the competing methods. It is seen that Itti's method, Hou's method, and Seo's method effectively detect region edges, but salient objects' inner regions are not effectively extracted. The graph-based method and the frequency tuned method extract the main parts of the salient regions, but they fail when salient objects occupy major part of the image or salient objects have colors similar to the background. Our method yields high saliency scores on both object's edges and inner regions, uniformly highlighting the entire salient regions from the background.

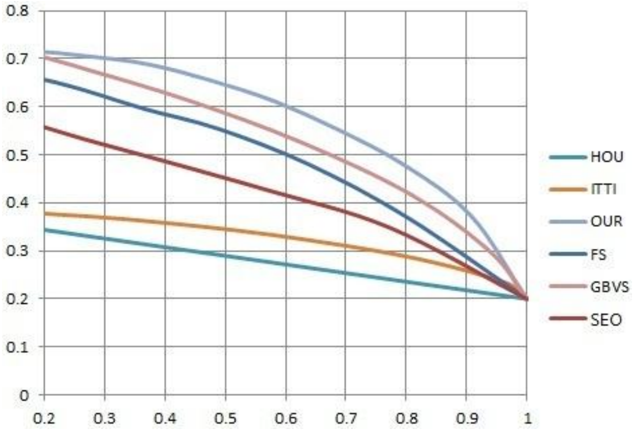

Fig. 13. Precision-recall curves.

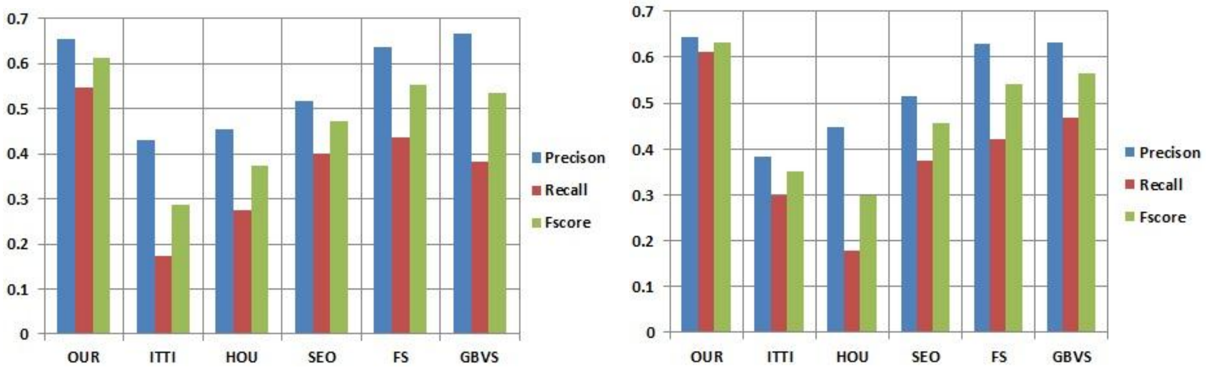

(a) (b)

Fig. 14. Precision-recall bars for binary saliency maps: The threshold *T* was determined using (a) Achanta's method and (b) Our method.

Fig. 13 shows the precision vs. recall curves of our method and the competing saliency detection methods by changing the value of the saliency threshold. It is seen that given the same recall, our method yields higher precision than the competing methods after transforming each original saliency map to a binary saliency map. Fig. 14 shows the values of the precision, recall and F measure of the saliency detection methods when Achanta's method and our method in (26) were used respectively to determine the threshold *T*. It is seen that our method yields the most accurate results no matter what the value of the threshold *T* was chosen, and the graph-based method and the frequency tuned method yield more accurate results than the other competing methods. It is apparent that our method more accurately separates the salient regions from the background. So, our anomaly detection method is effectively extended to image salience detection.

6. Conclusion

We have investigated local density-based anomaly detection. We have proposed a new kernel which is more appropriate for anomaly detection to estimate samples' local densities. We have also proposed the weighted neighborhood density estimation and shown that it is robust against variations in the size of the neighborhood. We have proposed a context-based local kernel regression estimator and a hierarchical combination strategy to combine the information from the multiple scale neighborhoods for both locally and globally refining the anomaly factors. We have applied the above anomaly detection methods to image saliency detection. We have proposed a kernel-based saliency score propagation method to combine visual contrast information and spatial distribution information. Our method has uniformly highlighted the entire salient regions according to its distribution information in the image. Experimental evaluations on the several datasets have demonstrated that our local kernel and weighted neighborhood density-based method is robust and efficient for anomaly detection and our hierarchical context-based kernel regression effectively refines anomaly factors. The effectiveness of our anomaly detection-based image saliency detection method has been validated by comparison with several state-of-art saliency detection methods.

References

1. F. Angiulli, R. B.-E.-Zohary, and L. Palopoli, "Outlier detection for simple default theories," *Artificial Intelligence*, vol. 174, no. 15, pp. 1247-1253, Oct. 2010.
2. M. Wu and J. Ye, "A small sphere and large margin approach for novelty detection using training data with outliers," *IEEE Trans. on Pattern Analysis and Machine Intelligence*, vol. 31, no. 11, pp. 2088-2092, Nov. 2009.
3. F. Angiulli, R. B.-E.-Zohary, and L. Palopoli, "Outlier detection using default reasoning," *Artificial Intelligence*, vol. 172, no. 16-17, pp. 1837-1872, Nov. 2008.
4. P.J. Rousseeuw and A.M. Leroy, "Robust regression and outlier detection," John Wiley and Sons, New York, 1987.
5. D. Hawkins, "Identification of outliers," Chapman and Hall, London, 1980.
6. B. Silverman, "Density estimation for statistics and data analysis," Chapman and Hall, London, 1986.
7. M.M. Breunig, H.-P. Kriegel, R.T. Ng, and J. Sander, "LOF: identifying density-based local outliers," *in Proc. of ACM SIGMOD International Conference on Management of Data*, pp. 93-104, 2000.
8. S. Papadimitriou, H. Kitagawa, and P. Gibbons, "LOCI: fast outlier detection using the local correlation integral," *in Proc. of International Conference on Data Engineering*, pp. 315-326, March 2003.
9. L.J. Latecki, A. Lazarevic, and D. Pokrajac, "Outlier detection with kernel density functions," *in Proc. of International Conference on Machine Learning and Data Mining in Pattern Recognition*, pp. 61-75, 2007.
10. J. Yang, N. Zhong, Y. Yao, and J. Wang, "Local peculiarity factor and its application in outlier detection," *in Proc. of ACM SIGKDD International Conference on Knowledge Discovery and Data Mining*, pp. 776-784, 2008.
11. J. Tang, Z. Chen, A.W.-C. Fu, and D.W. Cheung, "Enhancing effectiveness of outlier detections for low density patterns," *in Proc. of Pacific-Asia Conference on Advances in Knowledge Discovery and Data Mining*, pp. 535-548, 2002.
12. P. Sun and S. Chawla, "On local spatial outliers," *in Proc. of IEEE International Conference on Data Mining*, pp. 209-216, Nov. 2004.
13. A. Lazarevic and V. Kumar, "Feature bagging for outlier detection," *in Proc. of ACM SIGKDD International Conference on Knowledge Discovery in Data Mining*, pp. 157-166, 2005.
14. N. Abe, B. Zadrozny, and J. Langford, "Outlier detection by active learning," *in Proc. of ACM SIGKDD International Conference on Knowledge Discovery in Data Mining*, pp. 504-509, 2006.
15. L. Breiman, "Bagging predictors," *Machine Learning*, vol. 24, no. 2, pp. 123-140, Aug. 1996.
16. Y. Freund and R. Schapire, "A decision-theoretic generalization of on-line learning and an application to boosting," *Journal of Computer and System Science*, vol. 55, no. 1, pp. 119-139, Aug. 1997.
17. W. Jin, A. Tung, and J. Ha, "Mining top-n local outliers in large databases," *in Proc. of ACM SIGKDD International Conference*

on Knowledge Discovery in Data Mining, pp. 293-298, 2001.

18. J. Gao, W. Hu, Z. Zhang, and O. Wu, “Unsupervised ensemble learning for mining top-n outliers,” *in Proc. of Pacific-Asia Conference on Knowledge Discovery and Data Mining*, pp. 418-430, 2012.
19. V. Barnett and T. Lewis, “Outliers in statistic data,” John Wiley, New York, 1994.
20. J.L. Bentley, “Multidimensional binary search trees used for associative searching,” *Communications of the ACM*, vol. 18, no. 9, pp. 509-517, Sep. 1975.
21. E. Nadaraya, “On estimating regression,” *Teoriya Veroyatnoste i ee Primeneniya*, vol. 9, no. 1, pp. 157-159, 1964.
22. E. Knorr, R. Ng, and V. Tucakov, “Distance-based outliers: algorithms and applications,” *International Journal on Very Large Data Bases*, vol. 8, no.3- 4, pp. 237-253, Feb. 2000.
23. V. Jumutc and J.A.K. Suykens, “Multi-class supervised novelty detection,” *IEEE Trans. on Pattern Analysis and Machine Intelligence*, , vol. 36 , no. 12, 2510-2523, Dec. 2014.
24. R. Laxhammar and G. Falkman, “Online learning and sequential anomaly detection in trajectories,” *IEEE Tran. on Pattern Analysis and Machine Intelligence*, vol. 36, no. 6, pp. 1158-1173, June 2014.
25. D. Weinshall, A. Zweig, H. Hermansky, S. Kombrink, F.W. Ohl, J. Anemuller, J.-H. Bach, L.V. Gool, F. Nater, T. Pajdla, M. Havlena, and M. Pavel, “Beyond novelty detection: incongruent events, when general and specific classifiers disagree,” *IEEE Trans. on Pattern Analysis and Machine Intelligence*, vol. 34, no. 10, pp. 1886-1901, Oct. 2012.
26. G. Danuser and M. Stricker, “Parametric model fitting: from inlier characterization to outlier detection,” *IEEE Trans. Pattern Analysis and Machine Intelligence*, vol. 20, no. 3, pp. 263-280, Mar. 1998.
27. M. Markou and S. Singh, “A neural network-based novelty detection for image sequence analysis,” *IEEE Trans. Pattern Analysis and Machine Intelligence*, vol. 28, no. 10, pp. 1664-1677, Oct. 2006.
28. D.J. Miller and J. Browning, “A mixture model and EM-based algorithm for class discovery, robust classification, and outlier rejection in mixed labeled/unlabeled data sets,” *IEEE Trans. Pattern Analysis and Machine Intelligence*, vol. 25, no. 11, pp. 1468-1483, Nov. 2003.
29. T. M. Hospedales, J. Li, S. Gong, and T. Xian, “Identifying rare and subtle behaviours: a weakly supervised joint topic model,” *IEEE Trans. on Pattern Analysis and Machined Intelligence*, vol. 33, no. 12, pp. 2451-2464, Dec. 2011.
30. X. Song, M. Wu, C. Jermaine, and S. Ranka, “Conditional anomaly detection,” *IEEE Trans. on Knowledge and Data Engineering*, vol. 19, no. 5, pp. 631-645, May 2007.
31. H.S. Javitz and A. Valdes, “The SRI IDES statistical anomaly detector,” *in Proc. of IEEE Computer Society Symposium on Research in Security and Privacy*, pp. 316-326, May 1991.
32. M.J. Desforges, P.J. Jacob, and J.E. Cooper, “Applications of probability density estimation to the detection of abnormal conditions in engineering,” *in Proc. of Institute of Mechanical Engineers*, vol. 212, pp. 687-703, 1998.
33. H.E. Solberg and A. Lahti, “Detection of outliers in reference distributions: performance of Horn's algorithm,” *Clinical Chemistry*, vol. 51, no. 12, pp. 2326-32. Dec. 2005.
34. A. McCallum, D. Freitag, and F.C.N. Pereira, “Maximum entropy Markov models for information extraction and segmentation,” *in Proc. of International Conference on Machine Learning*, pp. 591-598, 2000.
35. E. Eskin, “Anomaly detection over noisy data using learned probability distributions,” *in Proc. of International Conference on Machine Learning*, pp. 255-262, 2000.
36. M. Otey, S. Parthasarathy, A. Ghoting, G. Li, S. Narravula, and D. Panda, “Towards NIC-based intrusion detection,” *in Proc. of ACM SIGKDD International Conference On Knowledge Discovery and Data Mining*, pp. 723-728, 2003.
37. D. Yu, G. Sheikholeslami, and A. Zhang, “Findout: finding outliers in very large datasets,” *Knowledge and Information Systems*, vol. 4, no. 4, pp. 387-412, Oct. 2002.
38. M.H. Arshad and P.K. Chan, “Identifying outliers via clustering for anomaly detection,” Technique Report, No. TR CS-2003-19, Department of Computer Sciences, Florida Institute of Technology Melbourne, FL 32901, pp. 1-8.
39. Z. He, X. Xu, and S. Deng, “Discovering cluster-based local outliers,” *Pattern Recognition Letters*, vol. 24, no. 9-10, pp. 1641-1650, June 2003.
40. M. Salehi, C. Leckie, and J.C. Bezdek, T. Vaithianathan, and X. Zhang “Fast memory efficient local outlier detection in data

streams," *IEEE Trans. on Knowledge and Data Engineering*, vol. 28, no. 12, pp. 3246-3260, Dec. 2016.

41. F.T. Liu, K.M. Ting, and Z.-H. Zhou, "Isolation forest," *in Proc. of IEEE International Conference on Data Mining*, pp. 413-422, 2008
42. L. Itti, C. Koch, and E. Niebur, "A model of saliency-based visual attention for rapid scene analysis," *IEEE Trans. on Pattern Analysis and Machine Intelligence*, vol. 20, no. 11, pp. 1254-1259, 1998.
43. X. Hou and L. Zhang, "Saliency detection: a spectral residual approach," *in Proc. of IEEE Conference on Computer Vision and Pattern Recognition*. pp. 1-8, June 2007.
44. H.J. Seo and P. Milanfar, "Static and space-time visual saliency detection by self-resemblance," *Journal of Vision*, vol. 9, no. 12, pp. 15-15, 2009.
45. J. Harel, C. Koch, and P. Perona, "Graph-based visual saliency," *in Proc. of Neural Information Processing Systems*, pp. 545-552, 2006.
46. R. Achanta, S. Hemami, F. Estrada, and S. Ssstrunk, "Frequency-tuned salient region detection," *in Proc. of IEEE Conference on Computer Vision and Pattern Recognition*, pp. 1597-1604, June 2009.
47. H. Jiang, J. Wang, Z. Yuan, Y. Wu, N. Zheng, and S. Li, "Salient object detection: a discriminative regional feature integration approach," *in Proc. of IEEE Conference on Computer Vision and Pattern Recognition*, pp. 2083-2090, 2013.
48. X.-H. Shen and Y. Wu, "A unified approach to salient object detection via low rank matrix recovery," *in Proc. of IEEE Conference on Computer Vision and Pattern Recognition*, pp. 853-860, 2012.
49. S. Goferman, L. Zelnik-Manor, and A. Tal, "Context-aware saliency detection," *in Proc. of IEEE Conference on Computer Vision and Pattern Recognition*, pp. 2376-2383, 2010.
50. M.M. Cheng, G.X. Zhang, N.J. Mitra, X.L. Huang, and S.M. Hu, "Global contrast based salient region detection," *in Proc. of IEEE Conference on Computer Vision and Pattern Recognition*, pp. 409-416, 2011.
51. G. Stein, B. Chen, A.S. Wu, and K. A. Hua, "Decision tree classifier for network intrusion detection with GA-based feature selection," *in Proc. of ACM annual Southeast regional conference*, vol. 2, pp. 136-141, 2005.
52. J.K. Dutta, B. Banerjee, and C.K. Reddy, "RODS: rarity based outlier detection in a sparse coding framework," *IEEE Trans. on Knowledge and Data Engineering*, vol. 28, no. 2, pp. 483-495, Feb. 2016.
53. C.-X. Ren, D.-Q. Dai, X. He, and H. Yan, "Sample weighting: an inherent approach for outlier suppressing discriminant analysis," *IEEE Trans. on Knowledge and Data Engineering*, vol. 27, no. 11, pp. 3070-3083, 2015.
54. M. Radovanovic, A. Nanopoulos, and M. Ivanović, "Reverse nearest neighbors in unsupervised distance-based outlier detection," *IEEE Trans. on Knowledge and Data Engineering*, vol. 27, no. 5, pp. 1369-1382, 2015.
55. C. O'Reilly, A. Gluhak, and M.A. Imran, "Adaptive anomaly detection with kernel eigenspace splitting and merging," *IEEE Trans. on Knowledge and Data Engineering*, vol. 27, no. 1, pp. 3-16, 2015.
56. E. Schubert, A. Zimek, and H.-P. Kriegel, "Generalized outlier detection with flexible kernel density estimates," *in Proc. of SIAM International Conference on Data Mining*, pp. 542-550, 2014.
57. E. Schubert, A. Zimek, and H.-P. Kriegel, "Fast and scalable outlier detection with approximate nearest neighbor ensembles," *in Proc. of International Conference on Database Systems for Advanced Applications*, vol. 2, pp. 19-36, 2015.
58. E. Schubert, M. Weiler, and A. Zimek, "Outlier detection and trend detection: two sides of the same coin," *in Proc. of IEEE International Conference on Data Mining Workshop*, pp. 40-46, 2015.
59. E. Schubert, A. Zimek, and H.-P. Kriegel, "Local outlier detection reconsidered: a generalized view on locality with applications to spatial, video, and network outlier detection," *Data Mining and Knowledge Discovery*, vol. 28, no. 1, pp. 190-237, 2014.
60. M. Ester, H.-P. Kriegel, J. Sander, and X. Xu, "A density-based algorithm for discovering clusters in large spatial databases with noise," *in Proc. of International Conference on Knowledge Discovery and Data Mining*, pp. 226-231, 1996.
61. H.-P. Kriegel, E. Schubert, and A. Zimek, "The (black) art of runtime evaluation: are we comparing algorithms or implementations?" *Knowledge and Information Systems*, vol. 52, no. 2, pp. 341-378, August 2017.
62. S. Pandit, D.H. Chau, S. Wang, and C. Faloutsos, "NetProbe: A fast and scalable system for fraud detection in online auction networks," *in Proc. of International World Wide Web Conference*, pp. 201-210, 2007.
63. D.H. Chau, C. Nachenberg, J. Wilhelm, A. Wright, and C. Faloutsos, "Polonium: Tera-scale graph mining and inference for

malware detection," *in Proc. of SIAM International Conference on Data Mining*, pp. 131-142, 2011.

64. W. Gatterbauer, S. Gunnemann, D. Koutra, and C. Faloutsos, "Linearized and single-pass belief propagation," *in Proc. of the VLDB Endowment*, vol. 8, no. 5, pp. 581-592, Jan. 2015.
65. N. Shah, A. Beutel, B. Hooi, L. Akoglu, S. Günnemann, D. Makhija, M. Kumar, and C. Faloutsos, "EdgeCentric: Anomaly detection in edge-attributed networks," *in Proc. of IEEE International Conference on Data Mining Workshops*, pp. 327-334, Dec. 2016.
66. Z. Li, X. Zhang, H. Shen, W. Liang, and Z. He, "A semi-supervised framework for social spammer detection," *in Proc. of Pacific-Asia Conference on Knowledge Discovery and Data Mining*, pp. 177-188, 2015.
67. X. Wu, Y. Dong, J. Tao, C. Huang, and N.V. Chawla, "Reliable fake review detection via modeling temporal and behavioral patterns," *in Proc. of IEEE International Conference on Big Data*, pp. 494-499, 2017.
68. Y. Yuan, G. Kaklamanos, and D. Hogrefe, "A novel semi-supervised Adaboost technique for network anomaly detection," *in Proc. of ACM International Conference on Modeling, Analysis and Simulation of Wireless and Mobile Systems*, pp. 111-114, 2016.

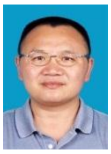

Weiming Hu received the Ph.D. degree from the department of computer science and engineering, Zhejiang University in 1998. From April 1998 to March 2000, he was a postdoctoral research fellow with the Institute of Computer Science and Technology, Peking University. Now he is a professor in the Institute of Automation, Chinese Academy of Sciences. His research interests are in visual motion analysis, recognition of web objectionable information, and network intrusion detection.

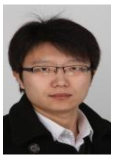

Jun Gao has a B.S. in Automation Engineering from BeiHang University, Beijing, China, and a Ph.D. in Computer Science from Institute of Automation, Chinese Academy of Sciences. His major research interests include machine learning, data mining, and network information security.

Bing Li received the PhD degree from the Department of Computer Science and Engineering, Beijing Jiaotong University, China, in 2009. Currently, he is an associate professor in the National Laboratory of Pattern Recognition (NLPR), Institute of Automation, Chinese Academy of Sciences. His research interests include color constancy, visual saliency and web content mining.

Ou Wu received the BS degree in Electrical Engineering from Xi'an Jiaotong University in 2003. He received the MS degree and PhD degree both from pattern recognition and machine intelligence from National Laboratory of Pattern Recognition (NLPR), Institute of Automation, Chinese Academy of Sciences in 2006 and 2011, respectively. Now, he is an Assistant Professor in NLPR. His research interests include information filtering, data mining, and web vision computing.

Junping Du received the Ph.D. degree in computer science from Beijing university of science and technology. She held a post-doctoral fellowship with the department of computer science, Tsinghua university, Beijing. She joined the school of computer science, Beijing university of posts and telecommunications, in 2006, where she is currently a professor of computer science. Her current research interests include artificial intelligence, data mining, intelligent management system development, and computer applications.

Stephen Maybank received a BA in Mathematics from King's college Cambridge in 1976 and a PhD in computer science from Birkbeck college, University of London in 1988. Now he is a professor in the Department of Computer Science and Information Systems, Birkbeck College. His research interests include the geometry of multiple images, camera calibration, visual surveillance etc.